
Article:
Wand, Charlie R. and Bates, Martin A. orcid.org/0000-0003-3482-3577 (2019) Chiral nematic liquid crystals in torus-shaped and cylindrical cavities. Physical Review E. 052702. ISSN 1550-2376

https://doi.org/10.1103/PhysRevE.100.052702

Chiral nematic liquid crystals in torus-shaped and cylindrical cavities

Charlie R. Wand* and Martin A. Bates
Department of Chemistry, University of York, Heslington, York YO10 5DD, United Kingdom

(Received 26 March 2019; published 25 November 2019)

We present a Monte Carlo simulation study of chiral nematic liquid crystals confined in torus-shaped and cylindrical cavities. For an achiral nematic with planar degenerate anchoring confined to a toroidal or cylindrical cavity, the ground state is defect free, with an untwisted director field. As chirality is introduced, the ground state remains defect free but the director field becomes twisted within the cavity. For homeotropic anchoring, the ground state for an achiral nematic within a toroidal cavity consists of two disclination rings, one large and one small, that follow the major circumference of the torus. As chirality is introduced and increased, this ground state becomes unstable with respect to twisted configurations. The closed nature of the toroidal cavity requires that only a half integer number of twists can be formed and this leads to the ground state being either a single disclination line that encircles the torus twice or a pair of intertwined disclination rings forming stable, knotted defect structures.

DOI: 10.1103/PhysRevE.100.052702

I. INTRODUCTION

The topological properties of ordered fluids such as nematic liquid crystals in confined geometries have received considerable attention in the past few decades because of the rich behavior that results from the frustration between the elastic energy of the bulk and surface energy imposed at the interface. Control of the geometry of the confined system, along with the molecular alignment at the interface, can lead to a fascinating and rich variety of director fields, including regions in which the orientational order characteristic of a liquid crystal vanishes, known as defects. This frustration occurs in even the simplest of oil-in-water type droplets, and so there has been a significant amount of work into understanding spherical droplets composed of liquid crystals with different types of surface anchoring [1–9]. Thin, curved but continuous surfaces such as nematic shells, which are double emulsions formed as water-in-oil-in-water type droplets, have also received interest and behave in a very different way due to the inner surface [10–17]. For systems with planar degenerate anchoring, the Poincaré-Hopf theorem [18] states that the total topological defect charge at each surface must be equal to the Euler characteristic of the system, given by $\chi = 2(1 - g)$ where g is the number of handles. The topological strength, s, of an individual defect is related to the rotation of the director around the defect; thus an $s = +1$ defect has a rotation in the director field of 2π. For a spherical surface (i.e., with no handles), $\chi = +2$, and therefore the total topological defect charge on the surface must also be equal to $+2$. Thin nematic shells are, therefore, predicted to have a total topological charge of $s = +2$ on both the inner and outer surface. This constraint can be satisfied by four $s = +1/2$ defects, or two $s = +1$ defects, or two $s = +1/2$ and one $s = +1$ defects in the ground state, depending on the conditions under which they are formed; in this case the defects are either disclination lines or escaped defects, which touch both inner and outer surfaces. Similar defects are also found at the surfaces of solid colloidal particles or nonmiscible droplets within a nematic host [19–24]. The induced interactions between the objects can lead to their self-assembly into chains or two-dimensional arrays [25–27] and disclinations in the nematic can be manipulated by the inclusions into exotic geometries such as knots [28,29]. The use of more complex-shaped colloidal particles, such as stars [30], toriods [31], colloids with handles [32], and knots [33,34], within a bulk nematic medium have also been investigated.

More complex curved cavities have been realized experimentally by Pairam *et al.* [35] and Ellis *et al.* [36]. Instead of a fluid medium for the outer phase, a gel matrix is used to stabilize nonspherical cavities. A nonspherical cavity, such as a torus, can be generated using a moving injection point. These droplets are topologically distinct from a sphere in that it is not possible to continuously transform between them without breaking the system. Nematic ordering on the surface of a toroid has been investigated theoretically [37–46] and a spontaneous twisted director configuration has been found leading to the breaking of achiral symmetry. This twisted director configuration has been observed experimentally [47] within nematic toroidal droplets with planar anchoring and also for DNA packing [48,49] and polymer bundles [50], both of which have been analyzed using liquid crystalline theory. Theoretical research by Koning *et al.* [51] and Pedrini and Virga [52] predict a transition from an untwisted to twisted director configuration dependent on the aspect ratio of the toroidal droplet and ratio of the Frank elastic constants of the liquid crystalline material. More recently nematic tori with homeotropic anchoring have also been investigated [36,53] and the geometric control of spontaneous twist

*Present address: Department of Chemical Engineering and Analytical Science, The University of Manchester, Oxford Road, Manchester M13 9PL, United Kingdom; c.wand@st-hildas.oxon.org; charlie.wand@manchester.ac.uk

considered including the possibility of forming interlinked disclinations.

In this paper, we investigate whether using a chiral nematic instead of an achiral nematic can stabilize chiral director configurations and thus form the intertwined disclinations as the ground state. This will provide a reliable way to produce these knotted defect structures. Coupled with the templating ability of the disclination lines [54], this provides a facile route for the synthesis of exotic nanoscale structures including interlinked rings and trefoil knots.

II. MODEL AND SIMULATION DETAILS

Monte Carlo (MC) simulations are used to investigate the behavior of both chiral and achiral nematic phases inside toroidal cavities. We use a coarse-grained model [15] in which a small volume of liquid crystal (LC) is modelled via an orientation dependent potential,

$$U^{\mathrm{LC-LC}}(\boldsymbol{p}_i, \boldsymbol{p}_j, \boldsymbol{r}_{ij}) = \begin{cases} r \leqslant \sigma, & \infty \\ \sigma < r < \sigma', & U^{\mathrm{LC-LC}}(\hat{\boldsymbol{p}}_i, \hat{\boldsymbol{p}}_j, \hat{\boldsymbol{r}}_{ij}), \\ \sigma' \leqslant r, & 0 \end{cases} \tag{1}$$

based upon a hard sphere of diameter σ, surrounded by an orientation dependent attractive region which has a further range of $\sigma' - \sigma$; in all simulations, $\sigma' = 1.5\sigma$. The unit vectors $\hat{\boldsymbol{p}}_i$ and $\hat{\boldsymbol{p}}_j$ denote the orientations of particles i and j and $\boldsymbol{r}_{ij} = |\boldsymbol{r}_{ij}|\hat{\boldsymbol{r}}_{ij} = r\hat{\boldsymbol{r}}_{ij}$ is the interparticle vector. The use of an off-lattice model overcomes the influence of the underlying lattice that influences the alignment in lattice-based models [24]. The anisotropic term which imposes the liquid crystal ordering is

$$\begin{aligned} &U^{\mathrm{LC-LC}}(\hat{\boldsymbol{p}}_i, \hat{\boldsymbol{p}}_j, \hat{\boldsymbol{r}}_{ij}) \\ &\quad = -\varepsilon(\hat{\boldsymbol{p}}_i \cdot \hat{\boldsymbol{p}}_j)^2 - \varepsilon_c[\hat{\boldsymbol{r}}_{ij} \cdot (\hat{\boldsymbol{p}}_i \times \hat{\boldsymbol{p}}_j)][(\hat{\boldsymbol{p}}_i \cdot \hat{\boldsymbol{p}}_j)], \end{aligned} \tag{2}$$

in which the first term is responsible for the nematic ordering and the second term introduces chirality; the strength parameters ε and ε_c correspond to the relative strengths of these two terms. Energies and derived quantities are quoted using ε as the scaling variable; thus temperature is scaled as $T^* = kT/\varepsilon$. Similarly, σ is used as the scaling variable for all distances. The molecular chirality can be varied through the parameter ε_c and the pitch length as a function of ε_c has previously been calculated for this model [15]. The bulk elastic constants were calculated for this model from bulk simulations using the method detailed by Allen *et al.* [55]. It was found that $K_1/K_3 = 1.038$ and $K_2/K_3 = 0.985$ where K_1, K_2, K_3 are the splay, twist, and bend Frank elastic constants, respectively. Indeed, due to the microscopic size of the toroidal droplets in question, each sphere represents an (undefined) number of mesogens, rather than a one-to-one mapping as, for example, in the Gay-Berne ellipsoidal model [56,57]. The level of coarse graining within this model allows for general features of the nematic phase to be captured.

The model liquid crystal is confined to either a toroidal or cylindrical cavity. A torus can be obtained by moving a sphere with a radius of r_c^* along a ring with a radius of r_t^*. The aspect ratio is defined as r_t^*/r_c^*, and gives a measure of thickness, with small values corresponding to fat tori and larger values to thinner tori. A cylinder can be thought of as a torus in the limiting case of $r_t^* \to \infty$. In simulations with a cylindrical cavity, the cylinder is periodic in the z direction with a radius r_c^* and length l^*. The anchoring at the surfaces of these cavities is imposed by an anisotropic LC-wall interaction,

$$U^{\mathrm{LC-wall}}(\boldsymbol{p}_i, \boldsymbol{r}_{ij}) = \begin{cases} r \leqslant \sigma, & \infty \\ \sigma < r < \sigma', & \pm\varepsilon_A(\hat{\boldsymbol{p}}_i \cdot \hat{\boldsymbol{r}}_i)^2, \\ \sigma' \leqslant r, & 0 \end{cases} \tag{3}$$

where $\hat{\boldsymbol{r}}_i$ is the unit vector between the center of the particle and the minimum distance on the toroidal (or cylindrical) wall. With the positive sign, $U^{\mathrm{LC-wall}}$ corresponds to planar anchoring and with the negative sign to homeotropic anchoring. ε_A is the anchoring strength and although this can be varied, in practice there is very little dependence on it so long as it is large enough for strong anchoring and so $\varepsilon_A = \varepsilon$ is used throughout.

All simulations were run at a single fixed density $\rho^* = N\sigma^3/V = 0.75$, corresponding to a relatively dense liquid; this is approximately 80% of the density of the liquid at the freezing point for hard spheres [58]. Note, when determining the number of particles required from the density, only the volume accessible to particles is taken into account. Therefore, a tube of radius r_c is taken to have an effective radius of $r_c - \sigma$ as the particles cannot approach the wall any closer. Exploratory simulations to determine the behavior were typically started from isotropic configurations and run at $T^* = 0.90T_{NI}^*$, where $T_{NI}^* = 1.46$ is the bulk isotropic-nematic transition temperature at this density [15]. In some cases, further simulations started from idealized configurations were also run and are discussed later. Various different system sizes and temperatures were used, as outlined in the appropriate sections. As a rough guide to system sizes, the smallest simulations of toroids with dimensions $r_t^* = 30$ and $r_c^* = 10$ contain 35 975 particles and the largest with dimensions $r_t^* = 40$ and $r_c^* = 20$ contain 213 776 particles. Simulations were run using an in-house standard Metropolis method [59] MC code and trial moves consisted of random translations, rotations, or a combination of the two. An additional trial move randomizing a selected $\hat{\boldsymbol{p}}_i$ was employed to speed up the equilibration time. An acceptance ratio of between 0.4 and 0.6 was maintained. Simulations were run for 2.5×10^5 MC cycles (where a cycle is defined as N trial moves) to equilibrate with results collected over 1.8×10^5 production MC cycles for ten random number seeds.

A range of fixed values for the chirality parameter were used; $\varepsilon_c^* = \varepsilon_c/\varepsilon = 0.00, 0.06, 0.12, 0.18$, and 0.24. $\varepsilon_c^* = 0.00$ corresponds to an achiral nematic phase (with infinite pitch), and the pitch lengths for the remaining values are $p^* = 202, 101, 62$, and 48, respectively [15]. The pitch values are found to be independent of temperature, which can be related to the square-well nature of the model potential [60].

In order to determine the orientational order and identify the locations and types of defects, the technique developed by Callan-Jones *et al.* [61] was used. This has previously been used for similar studies of nematic shells for both on- and off-lattice models [12,15]. The simulation box is split into a three-dimensional grid of cells with sides 1.5σ and a Q-tensor calculated for each region. Note that although the grid is applied to the whole simulation box, the analysis is only

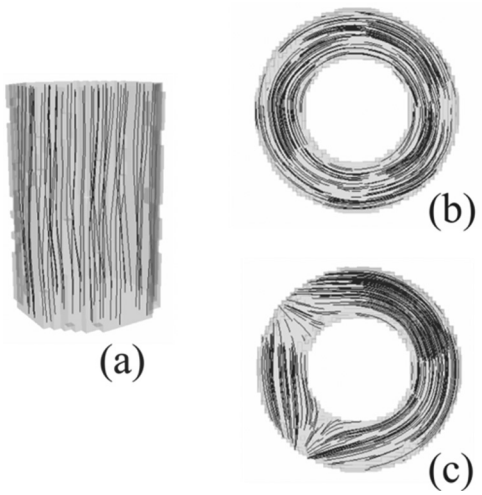

FIG. 1. (a) The director field for an achiral nematic ($\varepsilon_c^* = 0.00$) with planar anchoring inside a cylinder of dimensions $l^* = 48$, $r_c^* = 16$. (b) The director field in the defect-free ground state for a torus of dimensions $r_t^* = 28$, $r_c^* = 10$ and (c) in a higher energy metastable state with two pairs of boojum defects. Each boojum consists of a $s = +1$ defect on the outer waist of the surface and a $s = -1$ defect on the inner waist, giving a total surface topological charge of 0.

performed for those cells containing one or more particles. The Q-tensor

$$Q_{\alpha\beta}(r) = \frac{1}{N}\sum_{i=1}^{N}\left(p_{i\alpha}p_{i\beta} - \frac{1}{3}\delta_{\alpha\beta}\right), \tag{4}$$

where $\alpha, \beta = x, y, z$ and $\delta_{\alpha\beta}$ is the Kronecker delta, is calculated for each occupied cell and averaged over a number of configurations before being diagonalized. A modified version of the diagonalized Q-tensor, given by $D_{\text{diag}} = Q_{\text{diag}} + \frac{1}{3}I$, is used and has the eigenvalues $\lambda_1 \geqslant \lambda_2 \geqslant \lambda_3$ and $\lambda_1 + \lambda_2 + \lambda_3 = 1$ from which the relevant Westin metrics can be defined. The metric of most interest here is $c_l = \lambda_1 - \lambda_2$, which gives a measure of the local orientational order where $c_l = 1$ corresponds to perfect order and $c_l = 0$ to an isotropic state. Defects are defined as regions with $c_l \leqslant 0.15$. Preliminary simulations confirmed that the analysis grid and threshold values employed were suitable to accurately detect the defects.

The local director can also be visualized, using stream lines whose trajectory sweeps along the eigenvector field corresponding to λ_1, starting from random points chosen so that the streams pass throughout the liquid crystalline region. The visualizations were created using PARAVIEW 3.10.1 [62].

III. RESULTS AND DISCUSSION

A. Confined nematics and chiral nematics with planar anchoring

For liquid crystals in cavities with planar anchoring, the total topological charge at the surface is equal to χ, which is zero for both toroidal and (infinite) cylindrical cavities. For achiral nematics ($\varepsilon_c^* = 0.00$), the ground state in both types of cavity is expected to be defect free. This is indeed the case, as shown in Fig. 1, for all sizes of cylindrical and toroidal cavities studied. For the cylinder, a defect-free configuration is observed in which the director is parallel to the cylinder axis throughout the cylinder [Fig. 1(a)] while for the toroid, the director follows the major circumference of the torus [Fig. 1(b)]. For the toroidal cavities, higher energy metastable states are occasionally observed in which pairs of $s = +1$ and $s = -1$ defects form at the inner and outer surfaces [Fig. 1(c)]. The probability of these defects forming depends on the dimensions of the torus and on the cooling rate.

The director was found to follow the major circumference throughout the volume in the lowest energy state of all toroidal cavities investigated. The twisted director structure, as observed experimentally by Pairam *et al.* [35] and investigated theoretically by Koning *et al.* [51], was not observed. This indicates that in all cases either the cavities investigated were too slender (i.e., aspect ratio too large) to demonstrate the twisted configuration or the ratio of elastic constants is too close to 1. Due to the reasonably wide range of values of aspect ratios investigated, it is probable that in this case it is the ratio of elastic constants that is responsible for the absence of the twisted director configuration. The ratio $\kappa = (K_2 - K_{24})/K_3$ [35,51] is responsible for the spontaneous twisting of the director with twisted configurations expected for $\kappa \leqslant 5r_c^2/16r_t^2$. This reduces to $0.985 - K_{24}/K_3$ in the case of this model giving the upper bound for K_{24}/K_3 as 0.846.

The similarity in the elastic constants could again be due to the lack of shape anisotropy in the basic particles. It has also been suggested by Kulic [48] and later by Pedrini and Virga [52] that the ratio K_2/K_3 is important for explaining the presence of a twisted director configuration as, for many mesogens, particularly chromonic systems have $K_2 < K_3$ and the higher energy bend distortion around the torus is minimized by transforming to a lower energy twist distortion instead. Again, the simulation results are also consistent with this theory, as $K_2 \approx K_3$ there is no energetic reason to form the twisted director configuration.

To confirm that the untwisted director configuration is favored for the achiral nematic inside a toroidal cavity, simulations were run in which a local field was added to perturb the director into a twisted state. A local set of axes was defined such that $\boldsymbol{r}$ is a vector between the point of interest and the closest point on the major circumference, $\hat{\boldsymbol{s}}$, is a unit vector tangential to the major circumference of the torus and $\hat{\boldsymbol{t}}$ (parallel to $\hat{\boldsymbol{s}} \times \boldsymbol{r}$) is a unit vector tangential to the minor circumference. A local field

$$E_t = \varepsilon_f\left[\hat{\boldsymbol{s}}\left(1 - \xi_t\frac{r_i}{r_c}\right) + \hat{\boldsymbol{t}}\left(\xi_t\frac{r_i}{r_c}\right)\right] \tag{5}$$

is then applied to particle i, in which ε_f is the field strength and ξ_t is variable between 0 and 1; r_i is the distance between the particle and the major circumference. For $\xi_t = 0$, the resulting director follows the major circumference throughout the torus, whereas for $\xi_t = 1$, the director follows the major circumference only at the center of the tubular volume ($\boldsymbol{r} = \boldsymbol{0}$) and twists as $\boldsymbol{r}$ tends towards the outer edge of the torus [see Figs. 2(a) and 2(b)] in a double twist arrangement. A series of simulations are then run in which the value of ξ_t is then fixed while ε_f is varied and the average energy, including the aligning field, determined. A linear relationship is observed on increasing ε_f for all values of ξ_t [Fig. 2(c)], and so it is straightforward to extrapolate back to zero field, $\varepsilon_f = 0$,

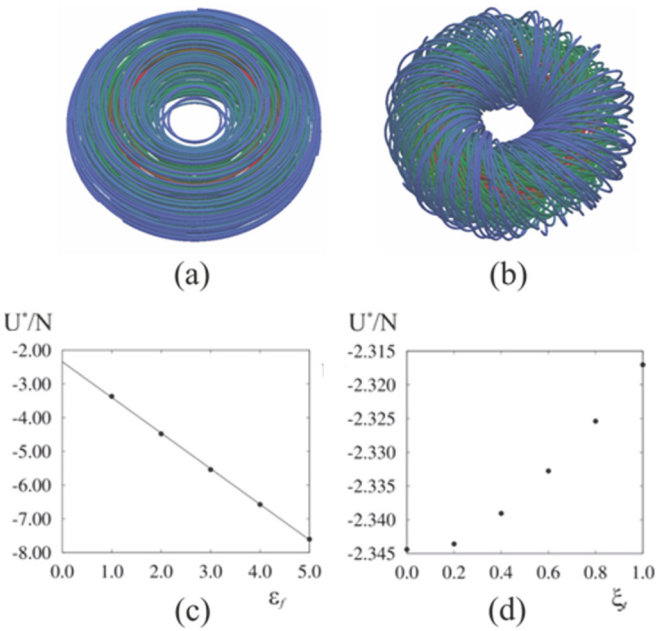

FIG. 2. Orientation of the aligning field in a torus of dimensions $r_t^* = 30$, $r_c^* = 20$ when (a) $\xi_t = 0.0$ and (b) $\xi_t = 1.0$. Streamlines at the center of the tube are colored red, then become green, then blue as the surface is approached. (c) Average energy per particle as a function of field strength ε_f for $\xi_t = 0.0$; the line indicates the best fit, with the extrapolation to zero field, $\varepsilon_f = 0.0$. (d) Average energy per particle, extrapolated to $\varepsilon_f = 0.0$, as a function of the imposed twist ξ_t.

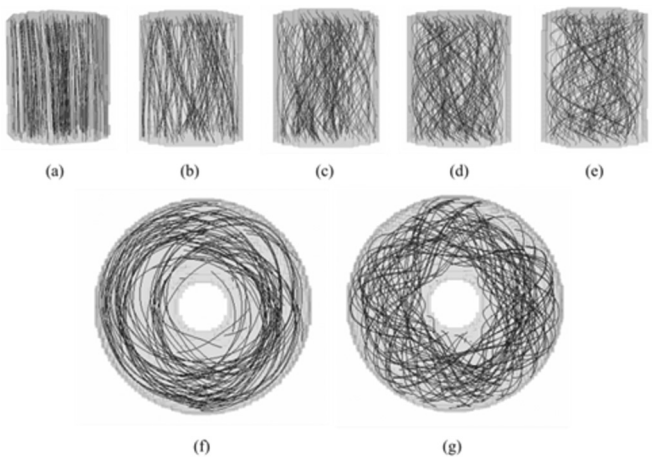

FIG. 3. Chiral nematics with planar anchoring inside a cylinder of dimensions $l^* = 36$, $r_c^* = 16$ with ε_c^* equal to (a) 0.00, (b) 0.06, (c) 0.12, (d) 0.18, and (e) 0.24. A torus of dimensions $r_t^* = 30$, $r_c^* = 20$ with ε_c^* equal to (f) 0.06 and (g) 0.18.

to give a measure of the configurational energy when the director is twisted but with the field turned off. A plot of the average energy against the amount of twist ξ_t [Fig. 2(d)] reveals that the minimum energy occurs for $\xi_t = 0$, i.e., the untwisted state. Thus we can be certain that the untwisted state is the ground state for this model. Similarly, the final configurations with the director twist induced by the field are found to become untwisted if further simulations are run with $\varepsilon_f = 0$, again indicating that the twisted director is not stable.

Although the achiral model nematic does not exhibit the doubly twisted director configuration, a twisted director configuration spontaneously forms for both cylindrical and toroidal cavities for chiral models ($\varepsilon_c^* \neq 0.00$), with the observed twist increasing with ε_c^*. For the cylindrical cavity, the director follows the cylinder axis at the center of the cylinder [Figs. 3(a)–3(e)], as in the achiral nematic case. However, as the distance from the center of the cylinder is increased, the director twists away from the cylinder axis. For the highest chirality ($\varepsilon_c^* = 0.24$) inside a cylinder of radius $r_c^* = 16$, the director at the edge of the tube is becoming almost perpendicular to that in the center; the angle is approximately 70°. Note that if it was truly perpendicular, this would be equivalent to a one quarter twist (through an angle of 90°). Since the pitch length for this model is $p^* = 48$, we might expect this rotation in the director to occur for significantly narrower tubes. Thus for the confined chiral nematic, the apparent pitch length is larger than expected.

An analogous director configuration is observed in the case of chiral nematics within toroidal cavities with planar anchoring, with the director at the center of the torus following the major circumference and twisting away from this as the surfaces are approached [Figs. 3(f) and 3(g)]. As expected, a greater twist is observed for thicker toroids (larger r_c^*) than for thinner ones (smaller r_c^*) although this is essentially independent of the major circumference (r_t^*). Thus the orientation of the director at the surface is similar for both toroids and cylinders of the same minor radius (and the same chirality liquid crystal) and hence the bend of the torus has little effect.

B. Confined nematics and chiral nematics with homeotropic anchoring

It is geometrically impossible to form an undistorted director configuration in a nematic liquid crystal inside a long cylindrical or toroidal cavity when there is strong homeotropic anchoring. The perpendicular surface alignment in a tubular geometry forces the ground state to be either two $s = +1/2$ disclination lines parallel to the tubular axis, one $s = +1$ disclination line, or one $s = +1$ escaped defect. In the former two cases, the director at any point is perpendicular to the (local) tube axis. For the escaped configuration, the director is perpendicular to the cylinder axis at the walls, but parallel to it in the center of the tube. The $s = +1$ disclination line tends to be found in narrow capillaries or close to the nematic-isotropic transition, but is unstable with respect to two $s = +1/2$ disclination lines as the radius increases as the energy of a disclination is proportional to s^2 [63]. For large radii, the escaped director configuration is most stable; however, it is very rarely observed, and instead a periodic array of defects with partially escaped domains between the defects is frequently observed [36,53,64,65]. Indeed, Ellis *et al.* [36] find either an escaped radial or twisted escaped radial defect configuration in nematic tori with 5CB and homeotropic anchoring.

For all simulations using the achiral nematic model ($\varepsilon_c^* = 0.00$) in cylinders or toroidal cavities with homeotropic anchoring, the ground state was found to be the configuration with two $s = +1/2$ disclination lines (Fig. 4). In the case of cylindrically confined nematics with homeotropic anchoring

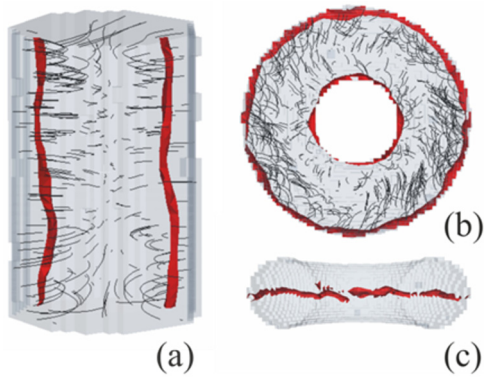

FIG. 4. (a) An achiral nematic with homeotropic anchoring inside a cylinder of dimensions $l^* = 48$, $r_c^* = 16$ and (b) inside a torus of dimensions $r_t^* = 30$, $r_c^* = 15$. (c) A cut-through view of the torus, showing the planarity of the disclination rings.

when $\varepsilon_c^* > 0.00$ the two $s = +1/2$ disclination lines twist around the cylinder to preserve both the chiral nematic helical twist and the homeotropic anchoring conditions (Fig. 5). Similar defect configurations have been reported experimentally for chiral nematic phases confined in capillaries [66,67]. Due to the periodic boundary conditions employed in these simulations, it is only possible for the disclination lines to form an integer number of half twists, $\xi = n/2$, where ξ is the number of full twists and n is an integer. This ensures that the director meets itself continuously at the boundary. Note that the twist observed for the homeotropic anchoring is along the axial direction of the cylinder, while for the previously mentioned cylinders with planar anchoring it is in the radial direction.

Preliminary simulations of cylindrical cavities in which the chiral nematic was cooled from the isotropic phase found different amounts of twist for the same value of ε_c^* with different random number seeds. The range of twists observed indicates that there is a mismatch between the chosen tube length and the (unknown) repeat distance. There are several possible approaches to identify the repeat distance. For example, the length of the tube could be varied, with a simulation run for each length, and the average energy per particle plotted as a function of the length. Minima in the average energy would occur when the tube length was equal to a half integer multiple of the repeat distance with the energy increasing as the length deviates from an optimal value. Jumps in the amount of twist observed would also be expected as a function of length. Alternatively, a fixed length cylinder could be used and the angle at which the boundaries join used as a variable during the simulation; again the system should reach an energy minimum when the twist at the boundary satisfies the twist required in the fixed length tube.

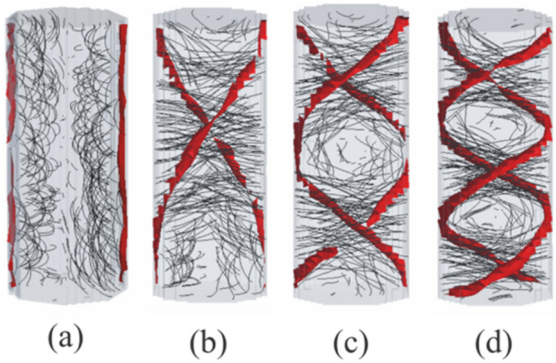

FIG. 5. Representative configuration for chiral nematics with homeotropic anchoring inside cylindrical cavities of dimensions $l^* = 96$, $r_c^* = 16$ with (a) $\xi = 0.0$, (b) $\xi = 0.5$, (c) $\xi = 1.0$, and (d) $\xi = 1.5$.

Here we take a slightly different approach based on idealized starting configurations based on a well-defined amount of twist within the cylinder (Fig. 5) and vary the length of the tube, or fix the length and vary the amount of twist. These simulations are relatively efficient, since long equilibration times to form the chiral nematic phase for each chiral model (differing in ε_c^*) are not necessary as we have well-defined twisted configurations for which the average energy needs to be determined. These simulations were necessarily run at a lower temperature of $T^* = 0.75T_{NI}^*$, as many of the higher energy configurations were no longer stable at the higher temperature of $T^* = 0.9T_{NI}^*$ and transformed into a more stable neighboring state. Presumably at lower temperatures, the thermal energy is not large enough to overcome the barriers between the states. It is also important to note that, for the chiral model used here, the bulk pitch length is found to be independent of the temperature, which can be related to the square-well nature of the potential [60] and therefore the pitch lengths for the higher temperature data can be used for comparison. We investigated two series, one with a fixed $r_c^* = 16$ with $l^* = 24, 36, 48, 72, 96$ [Figs. 6(a)], the other with fixed $l^* = 48$ for $r_c^* = 12, 16, 20$ [Figs. 6(b)] for all values of $\varepsilon_c^* = 0.00, 0.06, 0.12, 0.18, 0.24$.

In the case of a fixed l^* and r_c^* the amount of twist at the interpolated minimum average energy can be estimated by fitting a parabola to the data [Figs. 6(a) and 6(b)]. If two different twist values have similar energies, it is likely that they are either side of the optimal (but not possible) value; indeed, this is why multiple values of the twist can be found on cooling from the isotropic phase. Similarly, if the twist is fixed and the length varied, the length at which the average energy would have been a minimum can be estimated. The energy differences, especially on varying the radius of the cylinder, are relatively small and so quite a wide range of values are needed to be able to estimate the minimum.

Both series investigated give similar values of the repeat distance of the double helix as a function of ε_c^*, and the repeat distance decreases as ε_c^* increases, in the same way that the pitch of a chiral nematic phase decreases with increasing chirality. The repeat distance was found to be $1.45\times$ larger than the bulk pitch length for all the different values of ε_c^* studied [Fig. 6(c)]. Therefore it is clear that the homeotropic anchoring and the presence of the disclination lines in the cylinder weaken the effective chirality compared to in the bulk. This increase in pitch length is comparable to the experimental findings of Lequeux and Kleman [67] who found a twofold increase in pitch length in cholesterics confined in capillaries. We did not observe any dependence of the effective pitch length on r_c^* [Fig. 6(c)]. However, for all of these systems the diameter of the tube is smaller than the bulk

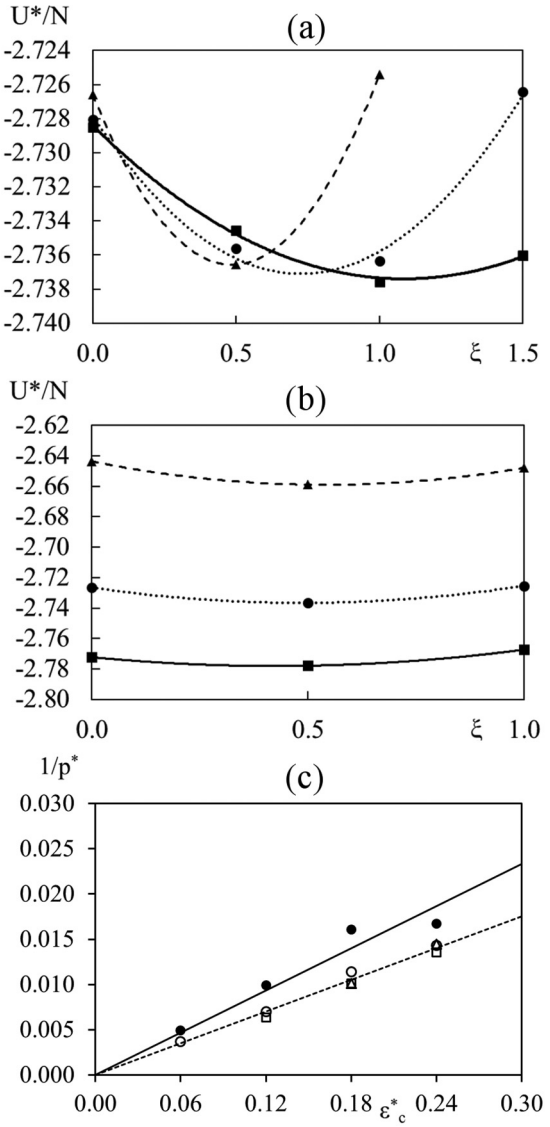

FIG. 6. (a) The average energy per particle as a function of ξ for $\varepsilon_c^* = 0.18$ for fixed $r_c^* = 16$, $l^* = 48$ (triangles, dashed line) $l^* = 72$ (circles, dotted line), and $l^* = 96$ (squares, solid line). (b) The average energy per particle as a function of ξ for $\varepsilon_c^* = 0.18$ for fixed $l^* = 48$, $r_c^* = 12$(triangles, dashed line), $r_c^* = 16$ (circles, dotted line) and $r_c^* = 20$ (squares, solid line). (c) The inverse of the pitch $(1/p^*)$ for the bulk chiral nematic (solid circles) and the inverse of the repeat distance for cylindrically confined systems as a function of chirality; data from all systems are investigated. The open symbols correspond to the cylindrically confined nematics with $l^* = 48$ (triangles), 72 (squares), 96 (circles), and $r_c^* = 16$. The solid line is a fit to the bulk pitch chiral nematic, while the dashed line is a fit to the combined chiral nematic cases.

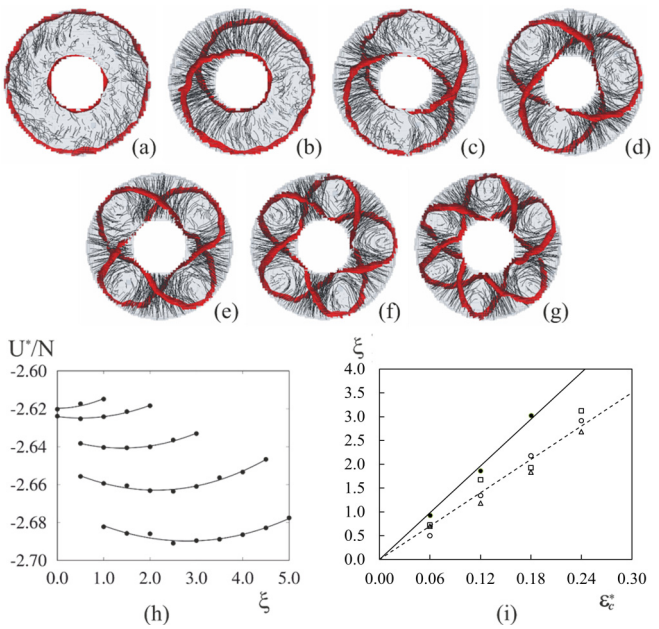

FIG. 7. Snapshots of the director field and disclination line(s) for chiral nematics with homeotropic anchoring inside a toroidal cavity of dimensions $r_t^* = 30$, $r_c^* = 15$ with ξ =(a) 0.0, (b) 0.5, (c) 1.0, (d) 1.5, (e) 2.0, (f) 2.5, and (g) 3.0. (h) The average energy per particle as a function of twist for $\varepsilon_c^* = 0.00$ to 0.24 (from top to bottom). (i) The expected twist (solid circles) based on the bulk pitch length $(2\pi r_t^*/p^*)$ and the actual twist in the toroidal cavity (open symbols); $r_t^* = 12$ (circles), 15 (squares), and 20 (triangles). The solid line is a fit to the bulk pitch length case, while the dashed line is a fit to the confined nematic cases.

pitch length; with these off-lattice models it is not possible to go to significantly large tube radii due to the large system sizes that would be required.

We extend the idea from cylindrical cavities with homeotropic anchoring to toroidal cavities. For a toroidal cavity, the "length" of the tube (that is, the distance traveled before the director has to be in phase with itself) is fixed and equal to the major circumference. Therefore, as with the cylinder simulations, an integer number of half twists, $\xi = n/2$, at the natural repeat distance may not fit exactly into the toroidal cavity. Of course, frustration is more likely when the major circumference is similar to or smaller than the natural pitch of the double helix.

A number of preliminary simulations were run at $T^* = 0.90T_{NI}^*$ for different sized toroidal cavities and values of ε_c^*, and various chiral states were observed. In general, the larger ε_c^*, the more twisted the disclination lines are. As for the fixed length cylinders, a more systematic series of simulations was then conducted at $T^* = 0.75T_{NI}^*$, starting from well-defined configurations for $r_c^* = 10$, 12, 15, 20 and the energy per particle is calculated. Representative configurations are shown in Figs. 7(a)–7(g). Note that unlike the case of the cylinder, here the circumference (and length) is fixed for a given r_t^*, and so only the amount of twist is varied in the starting configurations. Typical results for the average energy as a function of twist are shown for different values of ε_c^* in Fig. 7(h). Clearly, when $\varepsilon_c^* = 0.00$, the minimum occurs at zero twist, indicating that the configuration with two disclination rings in the plane of the torus is the ground state for the achiral model; if $\xi = 0.5$ or 1.0 then the elastic energy is increased. However, as the chirality is increased, the minimum in average energy shifts to larger twist values indicating that the ground state shifts from the planar pair of disclination rings, where the director has no twist around the circumference, to $\xi = 0.5$ in which a single disclination line traverses the toroidal cavity twice.

As ε_c^* continues to increase the lowest energy ξ also increases, with whole integer values of ξ formed of two disclination rings and half integer values of a single disclination ring. This dependence on ε_c^* means it should be possible to stabilize any of the twisted metastable states by tailoring the chirality of the chiral nematic [Fig. 7(i)]. Note that, as for the cylinders, changing the minor radius r_c appears to have no effect. As in the case of cylindrical confinement, the actual twist is below that expected from the bulk pitch length ($2\pi r_t^*/p^*$). Indeed, the actual twist is reduced by a factor of 1.45 compared to the expected value, in line with the value found for cylinders. Note that the pitch length in the toroidal droplets is taken as the lowest energy from a parabolic fit to the mean energy per particle for $0 \leqslant n \leqslant 5$ and as such it is not tied to half integer values of ξ. In the case of a toroidal cavity with homeotropic anchoring the splay elastic energy could be minimized by twisting the nematic causing the effective pitch length to deviate from that seen in the straight cylindrically confined case. However, for all values of r_c^* considered here the same effective pitch length was found.

IV. CONCLUSION

An off-lattice model has been used to investigate both achiral and chiral nematics inside cylindrical and toroidal cavities with either planar or homeotropic anchoring. For achiral nematics with planar anchoring, a defect-free untwisted director configuration is preferred. The twisted director configuration previously observed experimentally [35] and predicted theoretically [48,51] was not observed here, likely due to the similarity of K_1, K_2, K_3 which were found to be approximately equal in this model. Future work varying the Frank elastic constant ratios is needed to observe the transition from an untwisted to twisted director configuration which would allow for the measurement of K_{24}. Nevertheless, we are able to provide an upper bound for the ratio $\frac{K_{24}}{K_3}$ of 0.846.

However, a twisted director configuration was observed for chiral nematic systems, with the amount of twist observed increasing with increasing molecular chirality. This twisted director configuration can be observed for even the weakest chirality and hence the longest bulk pitch length studied, even though the pitch length is an order of magnitude larger than the dimensions of the torus.

For cylindrical and toroidal cavities with an achiral nematic with homeotropic anchoring, two $s = +1/2$ disclination lines were observed that run parallel to the tubular axis. The use of a chiral nematic causes these defect lines to twist about the axis and the amount of twist in the disclinations can be varied by varying the chirality of the nematic phase. Due to the topology of the toroidal cavity, the amount of twist (ξ) in the director field when traveling around the major circumference is necessarily a multiple of half integer twists so that the director is continuous. This leads to the disclinations forming torus knots or torus links, depending on whether the total twist is half integer or integer. In the case of half integers, a single disclination line is formed, which encircles the cavity twice before joining to itself, producing torus knot structures such as the trefoil or ($\xi = 1.5$) and cinquefoil ($\xi = 2.5$) knots. In contrast, when ξ is an integer, two distinct disclination lines form. In the simplest case of an achiral nematic, $\xi = 0$, the ground state has disclinations that lie in the plane of the torus and show no twist. However, with the introduction of chirality, the pair of disclination lines twist around each other ξ times forming linked circles and the disclinations can form linked structures such as the Hopf link ($\xi = 1$) consisting of a pair of circles linked once, a Solomon's knot ($\xi = 2$) where the pair of circles link twice, and so on. These findings highlight the importance of the confinement geometry and boundary conditions, demonstrating that more complex experimental approaches previously reported [28,29] are not necessarily required to controllably form knotted defect configurations. The simulations suggest that a tunable chiral nematic is used so that the chirality can be varied while the anchoring type and strength remain essentially constant. Therefore we can speculate that the most useful liquid crystal to use in such experiments is an achiral liquid crystal doped with varying amounts of a chiral dopant, to allow the chiral pitch to be continuously tuned.

ACKNOWLEDGMENTS

This research was supported by an EPSRC DTA Ph.D. Studentship. This research was performed while C.W. was at the Department of Chemistry, University of York, Heslington, York, YO10 5DD, United Kingdom.

There are no conflicts of interest to declare.

[1] J. Bezic and S. Zumer, Liq. Cryst. **11**, 593 (1992).
[2] F. Xu and P. P. Crooker, Phys. Rev. E **56**, 6853 (1997).
[3] T. C. Lubensky, D. Pettey, N. Currier, and H. Stark, Phys. Rev. E **57**, 610 (1998).
[4] M. Vennes and R. Zentel, Macromol. Chem. Phys. **205**, 2303 (2004).
[5] S. Sivakumar, J. K. Gupta, N. L. Abbott, and F. Caruso, Chem. Mater. **20**, 2063 (2008).
[6] M. A. Bates, J. Chem. Phys. **128**, 104707 (2008).
[7] T. Lopez-Leon and A. Fernandez-Nieves, Colloid Polym. Sci. **289**, 345 (2011).
[8] D. Sec, T. Porenta, M. Ravnik, and S. Zumer, Soft Matter **8**, 11982 (2012).
[9] F. Serra, Liq. Cryst. **43**, 1920 (2016).
[10] D. R. Nelson, Nano Lett. **2**, 1125 (2002).
[11] A. Fernandez-Nieves, V. Vitelli, A. S. Utada, D. R. Link, M. Marquez, D. R. Nelson, and D. A. Weitz, Phys. Rev. Lett. **99**, 157801 (2007).
[12] M. A. Bates, G. Skacej, and C. Zannoni, Soft Matter **6**, 655 (2010).
[13] T. Lopez-Leon, V. Koning, K. B. S. Devaiah, V. Vitelli, and A. Fernandez-Nieves, Nat. Phys. **7**, 391 (2011).
[14] V. Koning, T. Lopez-Leon, A. Fernandez-Nieves, and V. Vitelli, Soft Matter **9**, 4993 (2013).
[15] C. R. Wand and M. A. Bates, Phys. Rev. E **91**, 012502 (2015).

[16] T. Lopez-Leon, M. A. Bates, and A. Fernandez-Nieves, Phys. Rev. E **86**, 030702(R) (2012).
[17] S. Kralj, R. Rosso, and E. G. Virga, Soft Matter **7**, 670 (2011).
[18] O. D. Lavrentovich, Liq. Cryst. **24**, 117 (1998).
[19] H. Stark, Phys. Rep. **351**, 387 (2001).
[20] M. Ravnik and S. Zumer, Liq. Cryst. **36**, 1201 (2009).
[21] M. Tasinkevych, N. M. Silvestre, and M. M. Telo da Gama, New J. Phys. **14**, 073030 (2012).
[22] M. Cavallaro, M. A. Gharbi, D. A. Beller, S. Copar, Z. Shi, T. Baumgart, S. Yang, R. D. Kamien, and K. J. Stebe, Proc. Natl. Acad. Sci. USA **110**, 18804 (2013).
[23] S. Orlandi, E. Benini, I. Miglioli, D. R. Evans, V. Reshetnyak, and C. Zannoni, Phys. Chem. Chem. Phys. **18**, 2428 (2016).
[24] M. A. Bates, Liq. Cryst. **45**, 2390 (2018).
[25] P. M. Phillips, N. Mei, L. Reven, and A. Rey, Soft Matter **7**, 8592 (2011).
[26] Y. Kimura, K. Takahiro, K. Kita, and N. Kondo, J. Phys. Soc. Jpn. **81**, 084401 (2012).
[27] J. Dontabhaktuni, M. Ravnik, and S. Zumer, Soft Matter **8**, 1657 (2012).
[28] M. Humar, M. Ravnik, S. Pajk, and I. Musevic, Nat. Photon. **3**, 595 (2009).
[29] U. Tkalec, M. Ravnik, S. Copar, S. Zumer, and I. Musevic, Science **333**, 62 (2011).
[30] C. P. Lapointe, K. Mayoral, and T. G. Mason, Soft Matter **9**, 7843 (2013).
[31] M. Cavallaro, M. A. Gharbi, D. A. Beller, S. Copar, Z. Shi, R. D. Kamien, S. Yang, T. Baumgart, and K. J. Stebe, Soft Matter **9**, 9099 (2013).
[32] Q. K. Liu, B. Senyuk, M. Tasinkevych, and I. I. Smalyukh, Proc. Natl. Acad. Sci. USA **110**, 9231 (2013).
[33] Z. Kos and M. Ravnik, Soft Matter **12**, 1313 (2016).
[34] T. Machon and G. P. Alexander, Proc. Natl. Acad. Sci. USA **110**, 14174 (2013).
[35] E. Pairam, J. Vallamkondu, V. Koning, B. C. van Zuiden, P. W. Ellis, M. A. Bates, V. Vitelli, and A. Fernandez-Nieves, Proc. Natl. Acad. Sci. USA **110**, 9295 (2013).
[36] P. W. Ellis, K. Nayani, J. P. McInerney, D. Z. Rocklin, J. O. Park, M. Srinivasarao, E. A. Matsumoto, and A. Fernandez-Nieves, Phys. Rev. Lett. **121**, 247803 (2018).
[37] M. Bowick, D. R. Nelson, and A. Travesset, Phys. Rev. E **69**, 041102 (2004).
[38] L. Giomi and M. Bowick, Eur. Phys. J. E **27**, 275 (2008).
[39] L. Giomi and M. J. Bowick, Phys. Rev. E **78**, 010601(R) (2008).
[40] M. J. Bowick and L. Giomi, Adv. Phys. **58**, 449 (2009).
[41] R. L. B. Selinger, A. Konya, A. Travesset, and J. V. Selinger, J. Phys. Chem. B **115**, 13989 (2011).
[42] Z. W. Yao and M. O. de la Cruz, Phys. Rev. E **87**, 012603 (2013).
[43] Y. Li, H. Miao, H. R. Ma, and J. Z. Y. Chen, RSC Adv. **4**, 27471 (2014).
[44] A. Segatti, M. Snarski, and M. Veneroni, Phys. Rev. E **90**, 012501 (2014).
[45] D. Jesenek, S. Kralj, R. Rosso, and E. G. Virga, Soft Matter **11**, 2434 (2015).
[46] A. R. Fialho, N. R. Bernardino, N. M. Silvestre, and M. M. Telo da Gama, Phys. Rev. E **95**, 012702 (2017).
[47] I. I. Smalyukh, Y. Lansac, N. A. Clark, and R. P. Trivedi, Nat. Mater. **9**, 139 (2010).
[48] I. M. Kulic, D. Andrienko, and M. Deserno, Europhys. Lett. **67**, 418 (2004).
[49] H. Shin and G. M. Grason, EPL **96**, 36007 (2011).
[50] S. W. Ye, P. W. Zhang, and J. Z. Y. Chen, Soft Matter **12**, 5438 (2016).
[51] V. Koning, B. C. van Zuiden, R. D. Kamien, and V. Vitelli, Soft Matter **10**, 4192 (2014).
[52] A. Pedrini and E. G. Virga, Liq. Cryst. **45**, 2054 (2018).
[53] J. P. McInerney, P. W. Ellis, D. Z. Rocklin, A. Fernandez-Nieves, and E. A. Matsumoto, Soft Matter **15**, 1210 (2019).
[54] X. G. Wang, D. S. Miller, E. Bukusoglu, J. J. de Pablo, and N. L. Abbott, Nat. Mater. **15**, 106 (2016).
[55] M. P. Allen, M. A. Warren, M. R. Wilson, A. Sauron, and W. Smith, J. Chem. Phys. **105**, 2850 (1996).
[56] M. A. Bates and G. R. Luckhurst, J. Chem. Phys. **110**, 7087 (1999).
[57] D. J. Cleaver, C. M. Care, M. P. Allen, and M. P. Neal, Phys. Rev. E **54**, 559 (1996).
[58] E. G. Noya, C. Vega, and E. de Miguel, J. Chem. Phys. **128**, 154507 (2008).
[59] N. Metropolis, A. W. Rosenbluth, M. N. Rosenbluth, A. H. Teller, and E. Teller, J. Chem. Phys. **21**, 1087 (1953).
[60] C. R. Wand, Ph. D. thesis, The University of York, 2013.
[61] A. C. Callan-Jones, R. A. Pelcovits, V. A. Slavin, S. Zhang, D. H. Laidlaw, and G. B. Loriot, Phys. Rev. E **74**, 061701 (2006).
[62] J. Ahrens, B. Geveci, and C. Law, *PARAVIEW: An End-User Tool for Large Data Visualization*, in *The Visualization Handbook*, edited by C. Hansen and C. R. Johnson (Elsevier, Amsterdam, 2005).
[63] P. J. Collings and M. Hird, *Introduction to Liquid Crystals: Chemistry and Physics*, Liquid Crystal Book Series (CRC Press, Boca Raton, FL, 1997), pp. 1–41.
[64] G. De Luca and A. D. Rey, J. Chem. Phys. **127**, 104902 (2007).
[65] I. Vilfan, M. Vilfan, and S. Zumer, Phys. Rev. A **43**, 6875 (1991).
[66] P. E. Cladis, A. E. White, and W. F. Brinkman, J. Phys. (Paris) **40**, 325 (1979).
[67] F. Lequeux and M. Kleman, J. Phys. (Paris) **49**, 845 (1988).